Electronic structure of ordered silicon alloys: Direct-gap systems

Kurt A. Johnson and N. W. Ashcroft
Semiconductor Research Corporation and Laboratory of Atomic and Solid State Physics, Cornell University, Ithaca, New York 14853-2501

(Received 11 December 1995; revised manuscript received 20 February 1996)

Density functional theory (within the local density approximation) is applied to minimize the total energy of a set of Si/(group IV) ordered alloys and to calculate the associated electronic band structures. A series of fully relaxed Si/Sn alloys show direct gaps when constructed on the (100) surface of silicon in cubic-based superlattices, with the band gap of the Si/Sn alloys decreasing nearly linearly with increased atomic Sn fraction. Equivalent calculations performed with Ge and C substitutions are predicted to have direct and indirect gaps, respectively. Ternary alloys of Si/Ge/Sn and Si/Ge/C have band-structure features dominated by either the Sn or C substitutions having band gaps of the respective binary alloys. The magnitude of the conduction-band curvature (the effective mass) at the zone center of these alloys shows a strong variation dependent on the particular substitution. Energy barriers of the minor constituents are computed to estimate the stability of the binary alloys with resulting barriers near 0.25 eV for Sn and Ge atoms in a silicon matrix. [S0163-1829(96)07831-9]

I. INTRODUCTION

Silicon is the prime example of a semiconducting element, and it dominates the semiconductor industry. A significant reason for this dominance is silicon's well-established processing characteristics, which allow it to readily form insulating layers in device manufacturing. There is, nevertheless, a developing interest in finding a semiconductor for which the silicon processing technology can still be applied, but which has the added benefit of being a direct-gap material (silicon has an indirect gap with valence-band maximum at Γ and conduction-band minimum along the line Γ-X about 80% of the way to the zone edge).[1] A material with these properties could offer important applications in photoelectric devices, especially if it could be integrated with modern silicon devices using current processing technology. Relatively simple direct-gap materials exist of course; for example, GaAs is a commonly known direct-gap material but it lacks the favorable oxidation properties of silicon. Ordered semiconductor alloys provide a means for the creation of materials with new electronic characteristics such as smaller and larger band gaps or mobilities. One idea therefore is to work with semiconductor alloys that contain a large fraction of silicon, and search within this class for a direct-gap material. Through selection of the real space crystal structure we may hope to take advantage of band folding effects and bring the conduction-band minimum of silicon into the zone center, at Γ. We shall provide examples of such structures below, some of which also have reduced gaps.

Extensive studies have been performed on Si superlattices (SL's) with this intent, and Ge, as a second constituent, has probably received the greatest attention in this quest. Ge/Si alloys have been studied as both random mixtures and layered SL's.[2–6] Random alloys show little promise of achieving a direct gap; even a simple virtual crystal approximation (VCA) predicts an indirect gap[7] for all alloy mixtures. Further there is theoretical evidence that some SL structures produce direct-gap materials, for example, tight-binding calculations of 5×5 and 7×7 layered SL systems[5] grown on a (100) Ge substrate surface predict a resultant direct gap, but these direct-gap systems still pose the problem of low Si fractions due to the large Ge content. Other layered structures modeled on Si substrates have consistently produced indirect-gap materials that can be associated with Si conduction-band minima states that are not folded by the artificial layering process. This is true for both (100) and (111) SL structures examined with *ab initio*[2–4] and empirical methods.[5,6] SL systems grown as layered structures change the periodicity only in the growth direction resulting only in limited folding of the original Si bands back into the SL Brillouin zone (BZ). The periodicity of the SL unit cell along the surface remains commensurate with the underlying Si substrate, and many of the band minimum states will not be folded back into the new BZ. In other words the original indirect gap is left essentially unchanged. In fact, production of the direct-gap materials mentioned above arises primarily because of a combination of band folding in the growth direction and biaxial strain from the 4% lattice mismatch imposed on the Si by the Ge substrate. Work by Corkill and Cohen[8] and Edwards and Ashcroft[9] on hydrostatic stress on Si and Ge shows the conduction-band minima in Si can be raised relative to the lowest conduction state at the Γ state by such strain, even to the point of achieving a direct gap. Since the Si atomic layers in the Si/Ge SL's are under biaxial stress from the Ge substrate, Si band minima states along the surface direction are raised in energy above those states perpendicular to the growth surface.[3] The nonfolding X symmetry states are therefore no longer the minimum conduction-band states and the gap then moves to Γ, leaving a direct-gap material. It is evidently difficult to find a Si/Ge heterostructure of significant Si content with a direct gap.

However, as is well known, tin also comes in a semiconducting form (grey tin), which possesses the diamond structure. Si/Sn alloy gaps within the VCA exhibit a direct gap beyond 80% atomic tin compositions. Again the low silicon fraction is an evident technological problem in terms of pro-

cessing. With a lattice constant of 6.49 Å (Ref. 1) (compared to Si's 5.43 Å) tin has a significant lattice mismatch with silicon, and the ready formation of layered SL's with these materials is perhaps not expected. Recently, however, another style of SL system has been examined by Horsfield and Ashcroft.[10] These SL's are not composed of the typical alternating layer scheme of the Si/Ge SL's; but instead, the proposed alloy is formed from submonolayer deposition of tin onto a silicon surface creating an ordered surface reconstruction. Silicon is then grown on the partially filled surface to complete the layer and further growth continued, a technique that produces a larger unit cell both perpendicular and parallel to the growth surface. The original work consisted of theoretical SL's constructed on the (111) face of Si, and although no direct gaps were discovered, the band gap was consistently reduced by the addition of relatively small amounts of tin in the SL. The lack of a direct gap is straightforwardly explained by the band folding analysis (as discussed above), which occurs with these SL's grown on the Si(111) surface. The SL structures are hexagonal in real space (with hexagonal reciprocal space BZ's) tending to fold the silicon states with the L symmetry points into the center of the new BZ. The conduction-band minima of silicon, near X, are then likely to be translated near to the edge of the new BZ, still leaving an indirect material.

Proceeding with SL systems on Si, we now wish to look instead at the (100) face of Si, a natural extension from the (111) class. A number of elements have been deposited on Si(100) to produce ordered surface reconstructions including many group III metals for which the ordered phases of submonolayer structures have been mapped out quite extensively.[11,12] Tin has also been deposited onto the (100) surface, producing a variety of reconstructions for submonolayer coverages.[13,14] Of particular note are the $c(4\times4)$ reconstruction and the observation of regions of 2×2 ordering. These even valued surface orderings can produce simple cubic and tetragonal SL unit cells with the correct layering in the growth direction. By these means we expect to achieve a correct folding of the silicon bands through a judicious choice of real space unit-cell geometry. We also expect to keep a fair silicon fraction within the SL cell, which can easily be controlled through the choice of the number of pure silicon layers. Although tin receives the greatest attention, we examine below the electronic band structure of a number of Si/(group IV) ordered alloys in both binary and ternary forms.

In the context of practical utilization two concerns for any ordered SL are the issues of stability and formation of defects, and the ensuring effects of disorder on the bands. In Sec. III we provide estimates of the barriers holding our substitutional elements in place and calculate disorder effects through the coherent potential approximation (CPA) method.

II. METHOD

We apply density functional theory within the local density approximation (LDA) (Refs. 15 and 16) to the electronic structure problem associated with the proposed SL structures. The method employs a preconditioned conjugate gradient algorithm[17,18] to minimize the LDA total energy. *Ab initio* pseudopotentials with norm-[19] and hardness-conserving[20] properties replace the ion-electron interactions and are expected to provide good results in a variety of crystal environments. The LDA exchange-correlation energy is given by the Ceperley-Alder[21] result, and the crystal wave functions are expanded in a plane-wave basis set with a cutoff energy determined as discussed below. We are cognizant of the well-known LDA deficiency concerning band-gap calculations (the underestimate by 30%–50% of the experimental band gap in many semiconductors), but the resulting *trends* in these ordered SL alloys are expected to be valid for the true gaps as well (see discussion in Sec. IV).

For each ordered alloy a SL is chosen to represent the construction on the Si(100) surface, which are simple tetragonal, simple cubic, or body-centered tetragonal. Lattice constants along the growth surface are matched to silicon while the perpendicular lattice constant is determined by finding the value that minimizes the total energy of the SL. An energy cutoff of 20 Ry is used for this stage of the computation, and a few (2 or 4) **k** points were chosen according to a special point scheme.[22] Atoms within the SL are also systematically relaxed during this procedure, which includes essential structural changes in the SL potential. The algorithm accomplishes this task through an iterative process during which the atomic forces are calculated at each stage and the atoms moved along paths, which further minimize the energy. This process is repeated until the atomic forces are reduced beyond a preset limit, 3×10^{-4} hartrees/bohr, which produced bond lengths that changed by less than 1% in these systems compared to a limit of 3×10^{-3} hartrees/bohr. The structure is then considered fully relaxed for our purposes. The electron density of the relaxed structure is obtained from the equilibrium atomic positions with an energy cutoff of 40 Ry and a larger set of **k** points determined by the crystal symmetry.[23]

One exception is the class of carbon-based alloys; the strength of the carbon potential causes the greatest deformation of neighboring bond lengths and consequently the total energy calculation is computationally intensive. Because of this and from a careful survey of preliminary results (in particular the persistent occurrence of an indirect band gap), it was not deemed necessary to completely relax the carbon alloy structure. Certainly the value of the band gap will change further for the fully relaxed structure, but the main point is that the character of the band gap is unlikely to be altered because the difference between the LDA direct gap (0.32 eV) and indirect gap (0.01 eV) is significant. Spin-orbit splitting is not included in any of the calculations; it is most important in tin, but even then it is a small effect. The correction will not be significant for these silicon-rich alloys in which the tin fraction is small.

There are three main points in the BZ to be examined in assessing the new bands. First, we look at the point Γ, which contains new states folded from the old BZ. Second, the line along Γ-X of the silicon BZ is examined to assess how the original conduction-band minimum is altered with ordering of the alloy, particularly if it is folded into the zone center or onto the edge of the new BZ. Third, we look at what was originally the L symmetry point, which is either translated to the point M in the BZ of the tetragonal SL's systems, or not folded at all for the simple cubic SL. The point L is important because it possesses a lower-energy conduction-band

state than Γ in silicon and may be altered by the SL perturbation. Inspection of the bands and application of group theory in determining whether light can be directly coupled to new low-lying states gives us the character of the gap.

Once the band structure has been assessed for both band-gap value and character (direct or indirect), we proceed to an estimate of the stability of these alloys using the total-energy method. The minimized structure is formally *metastable* since it does not occur through normal thermodynamic mixing, and it is important to examine the barriers that constrain any diffusional motion of the substitutional atoms. Atoms in these structures are bonded in a tetrahedral structure, so the path of least energy would normally fall along the line that passes through the equilateral triangle formed by three of the nearest neighbors. Although the three silicon atoms do not strictly form an equilateral triangle because the minimized structure does not maintain the perfect diamond bonding angles, the end product is extremely close in all cases. In any event, the chosen atom is moved along such a path, and the total energy of the unit cell is calculated at various stages. For this component of the calculation only one **k** point at Γ is used to describe the electron density, which should serve to determine the energy *differences* at each point along the path. For small deviations the energy wells are quadratic as expected and acquire higher-order terms further from equilibrium. This well can be fit to a polynomial expression, and an energy barrier for defect formation then determined.

Defects, in this case a substitutional atom that has moved to an interstitial site, will invariably affect the band structure of these materials. We study disorder in these systems through the CPA, employing the method of Stroud and Ehrenreich[25] based on the local empirical pseudopotential method.[26] First we fit the band structure of the alloy's constituent species to their respective band structures (as found in Ref. 1). A VCA calculation is completed with the fitted potentials to get the bands of an unperturbed alloy and density of states needed for the CPA calculation. The density of states is determined using the tetrahedral method of Chen[27] using 318 **k** points in the irreducible part of the BZ, which are then interpolated on a grid 125 times as dense. The scattering potential is modeled by a square well with a radius equal to the average hard sphere packing radius of the two constituent species. This does not completely describe the real difference in potential between any two atoms used here, so the scattering strength is determined by taking an average of the difference of the empirical pseudopotential parameters as in Ref. 25. The CPA equations are solved with the iterative average T matrix technique[28] for energies in the upper half complex plane and analytically continued back to the real axis.[29] As we shall see, disorder effects are not large provided the alloy remains silicon rich, but an obvious physical requirement here is that corresponding mean free paths are large compared with the unit cell dimensions that establish the superlattice.

III. RESULTS

The approach we use in the choice of unit cell is geared towards producing an optimal folding of the Si bands into the center of a new BZ. An optimal folding is one that brings as many of the original six degenerate Si conduction-band minima as possible into the center of the new BZ. An obvious choice for the (100) surface is the simple tetragonal unit cell shown in Fig. 1(b) with Si atoms at their normal locations except for the substitution of other group IV elements at, for example, the center of the cell. Production of this unit cell requires a 2×2 half monolayer, ordered surface deposition onto the Si(100) surface, then the addition of 7 full Si monolayers, and repetition of the procedure. The BZ produced by this structure leads to a folding of the Si zone edge states from X, near the conduction-band minima, onto Γ. The bands will primarily resemble those of Si since the number of substitutions in the supercell is one group IV replacement for every 16 silicon atoms. Although we do not directly fold the minima into the zone center, we expect the perturbation of the SL potential, produced by the substitutional atoms and structural deformation, to split the folded, degenerate states. The splitting may depress some of the new folded states below the original Si minimum, an effect that was observed in the original Si/Sn (Ref. 10) work. With enough Sn atoms added to the unit cell such splitting at the new BZ edge caused these zone edge states to drop below the original band minimum states.

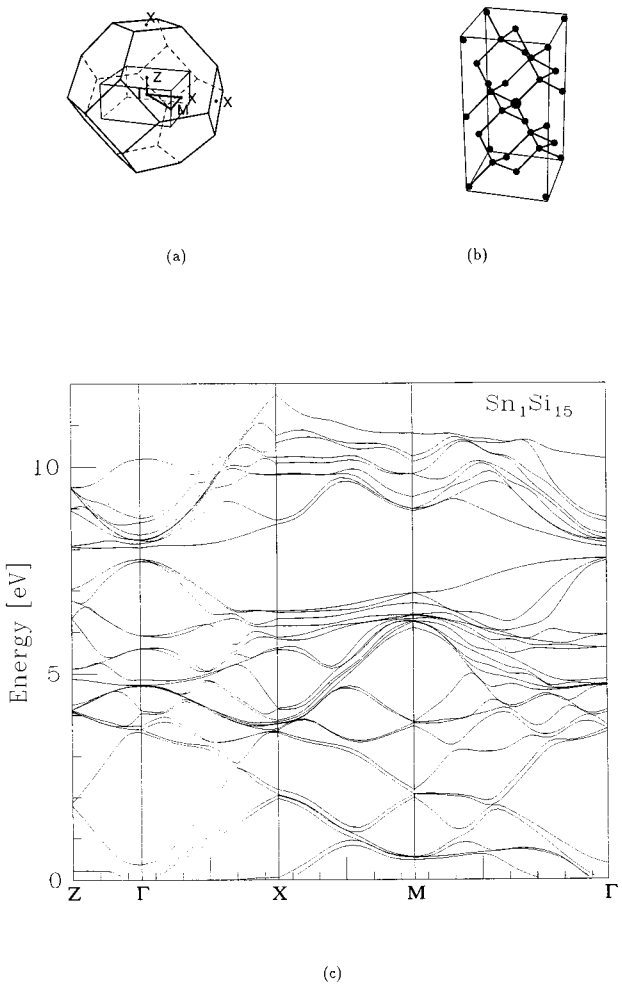

FIG. 1. Brillouin zone of the tetrahedral structures is shown in (a) with superlattice structure used for the Si/C, Si/Ge, and Si/Sn alloys with a ratio of 15 Si atoms to 1 group IV atom in (b). The large grey sphere corresponds to the substitutional atom. The electronic band structure of the Si(15)/Sn(1) alloy is given in (c).

A. Si/Sn ordered alloys

The band structure of the $Si_{15}Sn_1$ ordered alloy is shown in Fig. 1(c), which has the SL structure of Fig. 1(b). The geometry of the BZ associated with this SL, given in Fig. 1(a), indicates that bands from the X symmetry points in the original Si BZ are folded onto Γ from each coordinate direction. Bands along the perpendicular direction (in the direction of the SL growth) fold back twice, and parallel bands (i.e., those along the surface direction) fold back once. The lowest conduction band from Γ-Z is nearly flat because the multiple folding leaves the lowest-lying band composed of the original Si band region near the symmetry point X. This region of the Si conduction-band minimum is relatively flat initially. The degenerate X symmetry states of silicon folded onto Γ experience band repulsion, the splitting of this degeneracy, which leaves the lowest conduction band sloping upwards away from Γ. The relative strength of the band repulsion is quantified by the energy difference among the lowest six conduction-band states at Γ, being 0.31 eV. This splitting turns out to be stronger than that found in the Ge case examined in Sec. III B and is responsible for the final band curvature near these states being larger. States originally at the L symmetry point in the Si BZ are translated to M in the new BZ, but only two degenerate L symmetry states are folded onto M, and the splitting from band repulsion here is about 0.05 eV, significantly smaller than the splitting seen at Γ. Overall, the band gap is then *direct*.

For an ordered alloy with one tin atom in eight there exist two reasonable crystal structures. Simply taking the tetragonal unit cell of Fig. 1(b) and placing one tin atom at the top and bottom center position we achieve a simple cubic unit cell. This structure is imagined to be built just as the tetragonal structure with the exception of placing three silicon layers to every one ordered tin layer rather than seven. Another form achieving this silicon to tin ratio is depicted in Fig. 2(a). In this case the successive ordered tin layers are offset by half the lattice distance in both lateral directions creating a body-centered tetragonal unit cell. Both of these Si-Sn_1 structures could be produced in principle by a 2×2 tin deposition process and serve to show the importance of the ordering in these SL systems.

The simple cubic ordered alloy has a cubic reciprocal space BZ. This alloy experiences the folding of all six X symmetry states similar to the $Si_{15}Sn_1$ ordered alloy with each direction folded once, while the L symmetry states are not folded into the new BZ. The band structure for this alloy is not shown here, but the splitting caused by the perturbation of the SL potential is stronger in this system than in the $Si_{15}Sn_1$ case as one expects from a larger tin fraction. The energy difference among the lower conduction-band states at Γ is 0.65 eV (about twice that compared to the $Si_{15}Sn_1$ ordered alloy), and the bands disperse upward more steeply away from Γ, leaving again a direct gap.

The second form of this alloy, existing as a body-centered tetragonal unit cell, is shown in Fig. 2(a). The BZ of this structure is more complicated than the cubic structure, but we find that the two X symmetry states in the $\langle 100\rangle$ direction (along the imagined growth direction) are folded onto Γ, and the remaining four degenerate X states sit at the edge of the new BZ. The effect of band folding here is comparable to

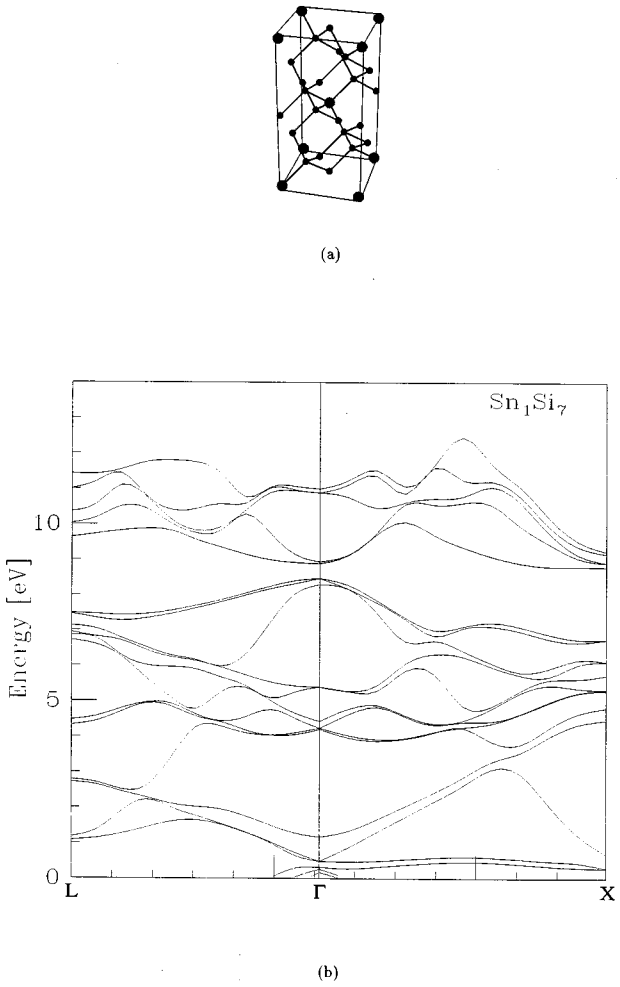

FIG. 2. One possible Si(7)/Sn(1) superlattice (a) with a body-centered tetragonal unit cell. Grey spheres indicate a substitutional atom. The band structure (b) shows an indirect gap at X.

many Si/Ge layered SL's in which the minimum conduction-band state remains located near X. For this alloy the band minimum actually moves out to the X symmetry point as observed for Si(111) based Si/Sn ordered alloys. When the original silicon symmetry is broken by the ordering process, the states at the zone edge are split, pushing the state at X below the original minimum. The two folded states at Γ exhibit minimal band repulsion (0.05 eV) that is much less than the splitting observed for the direct-gap alloy of the same tin fraction in which six degenerate states are folded. This is similar in magnitude to the splitting observed in the two degenerate L symmetry states, which were folded in the tetragonal ordered alloy.

A further set of Si/Sn alloys provides a sequence of band gaps versus tin concentration, so band structures for a Si_3Sn_1 and $Si_{13}Sn_3$ supercell have also been calculated although they are not shown; instead these results are simply summarized in Fig. 3, which shows the gap progression with results from the previous Si(111) work also included for completeness. For each distinct indirect alloy sequence, the band gap decreases almost linearly with the addition of tin. There are only three direct-gap alloys to examine, two of which have a near zero band gap. If we begin with pure

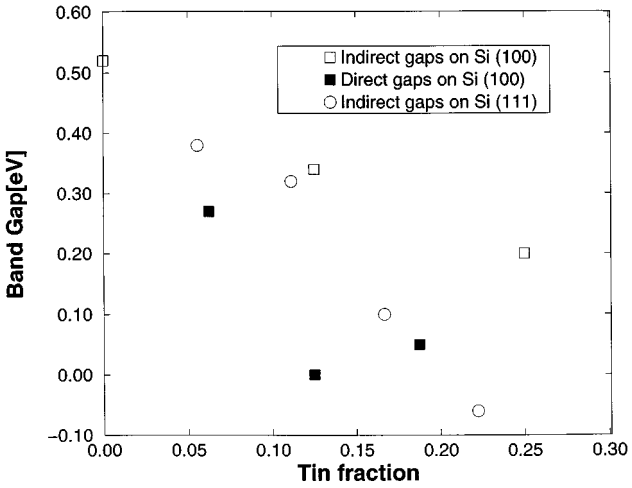

FIG. 3. Band gaps for all Si/Sn based alloys examined here. Normal Si in the diamond structure is shown at 0 tin fraction with a gap of 0.52 eV. Open circles indicate previous work on Si(111), open squares indicate indirect gaps for Si(100) SL's, and filled squares depict direct-gap SL's built on Si(100).

silicon, these gaps also proceed linearly with increased tin fraction up to the Si_7Sn_1 alloy, but the band gap of the Si_3Sn_1 alloy does not decrease below zero to maintain the linear relationship. It is well known that LDA calculations cannot successfully predict excited states such as the conduction bands, and we might therefore expect that a correction for these gaps would place then linearly much like the indirect gaps. The Si(111) calculations on the other hand could produce a negative gap because the conduction-band minimum falls at a location in k space way from the valence-band maximum at Γ, which allows the conduction-band minimum to sink below the valence-band maximum without any band crossing. It is unlikely that the ordered alloy with only 1 tin compared to 7 silicon atoms is metallic, so it is not easy to fully interpret the direct-gap results. We note that the direct gaps fall on a line consistently lower than indirect gaps of similar tin fraction. Recalling that direct-gap materials receive an additional reduction in gap magnitude through strong repulsion of folded states at Γ, this is to be expected.

B. Related group IV substitutions

Carbon and germanium SL's of the style shown in Fig. 1(b) were examined to determine the effect of other isoelectronic elements. Figure 4(a) shows the band structure of $Si_{15}Ge_1$. The lowest conduction bands near Γ are somewhat flatter than the tin alloy of similar constitution, which is readily explained by the weaker band repulsion of the folded states in this alloy. The six degenerate Si band-edge states folded from the point X are split by 0.21 eV, less than the comparable tin alloy. Therefore, the conduction-band states at Γ are less depressed, implying a weaker upward dispersion. We, of course, do not expect a significant perturbation from the Ge substitution. CPA calculations[7,25] predict very little band broadening from alloy scattering in random Si/Ge alloys, and the length of the Si-Ge bond in this relaxed alloy differs from the Si-Si bond length by only about 1%, so there is little chemical or structural deformation of the underlying

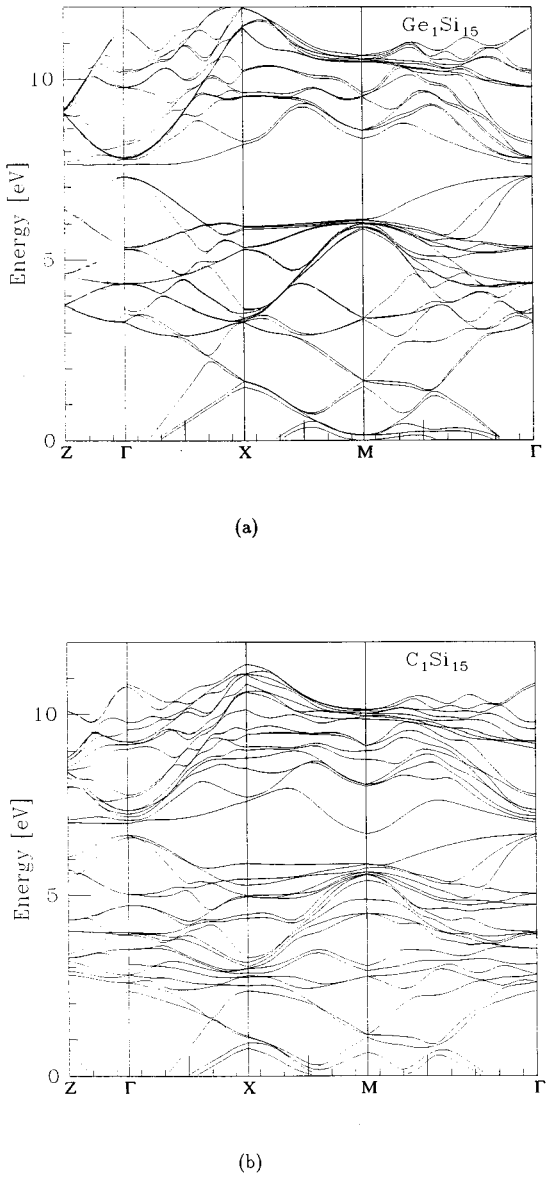

FIG. 4. Electronic band structure of the Si/Ge (a) and Si/C (b) alloys based on the SL of Fig. 1(b).

silicon matrix in this case. The band gap is just barely direct, unlike SiGe layered SL's on Si(100) in which fewer states are folded into the zone center.

The Si/C alloy based on the Fig. 1(b) SL exhibits a distinct band ordering at the M symmetry point unlike either the Si/Ge or Si/Sn ordered alloys. Figure 4(b) shows that the lowest conduction-band states at M are both nondegenerate, while the other binary alloys display a nondegenerate state followed by a double degenerate set of conduction-band states. More importantly the lowest conduction band along Γ-M reaches a minimum at the symmetry point M leaving the gap indirect. The conduction bands along Γ-Z are folded as in the previous ordered alloys showing the strongest splitting, 0.35 eV, and upward dispersion away from Γ of the $Si_{15}X_1$ binary ordered alloys because of the perturbation of the carbon potential both chemically and structurally. It may be noted that the M symmetry point in these BZ's contains states that originated at L in the original BZ. As mentioned

in the Introduction, SL alloys built on the (111) Si surface tend to fold states from L into the BZ, which suggests that a Si/C alloy on Si(111) may be promising. This state may also arise from a carbon state (forming an impurity type band) in the tight-binding sense, which would then negate the band folding argument.

Beyond these binary ordered alloys we can also imagine forming ternary SL compounds. It may be advantageous to work with ternary alloys in order to reduce strain in the SL by altering the offset of consecutive submonolayers (i.e., not placing each submonolayer directly in line with the previous one.) In terms of band-gap engineering, ternary alloys also offer greater flexibility for manipulating band-gap magnitudes and curvature. The SL's are styled as in Fig. 2(a) with the corner atoms replaced by one substitutional species and the central atom by the second substitutional species. In the case of a single substitutional species this SL produced a body-centered tetragonal unit cell and gave an indirect-gap material. In the ternary form we again create a tetragonal unit cell and produce significant band folding of Si minima states. Two examples of this type are $Si_{14}Ge_1Sn_1$ and $Si_{14}Ge_1C_1$. The Si/Ge/Sn alloy produces a direct gap similar to the $Si_{15}Ge_1$ and $Si_{15}Sn_1$ alloys while the Si/Ge/C alloy reveals the same indirect gap as the $Si_{15}C_1$ alloy, which is not shown. The Ge addition mainly contributes weakly to stronger dispersion of the bands near Γ.

C. Alloy defects

We have applied the total-energy algorithm to estimate defect formation energies. The nearest-neighbor distance from the substitutional atoms in the relaxed structures are 2.49, 2.37, and 2.07 Å for Sn, Ge, and C, respectively. The maximum barrier heights are 0.265, 0.242, and 0.11 eV occurring at distances of 1.18, 1.12, and 0.96 Å away from equilibrium. For reasonable temperatures we therefore expect the Sn and Ge barriers to be large enough to sufficiently contain them. Experimental work with Sn,[14] in which Sn was deposited on Si(100) and annealed at 500 °C, showed negligible movement of the Sn atoms into the underlying substrate from their bonding sites. The C atom obviously forms the strongest bonds with the Si atoms, drawing them within 2.07 Å, yet in these silicon-rich systems it has the lowest-energy barrier to shifting away from equilibrium. The reason is that the Si/C alloy is a more open structure than either the Ge or Sn types, which push the nearby Si atoms away (the normal Si-Si bond length is 2.35 Å). The carbon atom therefore has more space at the interstitial site to which it is being moved, and therefore is actually being pushed through a region of lower electron density, different from that expected in the ordered compound Si-C. Other carbon-based materials (i.e., 3C-SiC with a lattice constant of 4.36 Å,[1] almost 20% smaller than Si) would likely have higher barriers due to the larger electron density of the tightly packed atoms.

Figure 5 shows the band-gap shift and broadening for random Si/Sn alloys as calculated within the CPA. For systems with complete chemical disorder (random placement of the Si and Sn atoms on a diamond lattice), the broadening becomes significant for larger Sn fractions. We expect that an ordered alloy such as we have imagined constructing (with some small amount of disorder caused by defects in growth) would exhibit even less broadening of the band edge states than shown here. The defect barriers calculated above indicate that decomposition of the ordered lattice after construction would not be problematic for Ge and Sn substitutionals with the larger barriers and reasonable thermal energies. So a silicon-rich system has encouraging characteristics even in terms of disorder.

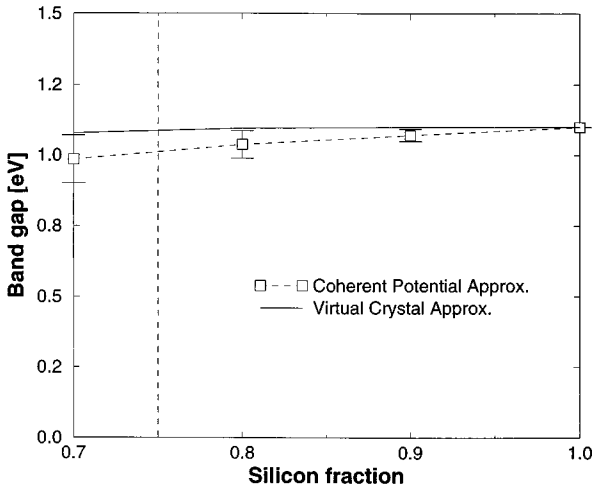

FIG. 5. Coherent potential approximation applied to random Si/Sn alloys. Error bars indicate broadening from incoherent scattering. Horizontal dashed line indicates the shift in the gap magnitude, and the vertical line separates the silicon-rich alloys studied here from those with greater atomic tin fractions.

IV. CONCLUSIONS

Clearly the focus is on band gaps, and it is precisely these quantities that are least well predicted by the local density approximation in the density functional theory. For example, LDA gives very good structural parameters for Si,[24] yet the predicted band gap is 0.52 eV,[30,31] some 0.65 eV below the experimentally determined value of 1.17 eV. Given this state of affairs there is some uncertainty about the *absolute* quantitative predictions we have given. Nevertheless it is important realize that the LDA can reproduce *trends* in the band structure fairly successfully.[32,33] We have shown, for example, that the band gap of the Si/Sn ordered alloys changes nearly linearly with increase in tin fraction (see the discussion above about the direct-gap results), and gaps of a direct nature are consistently smaller than indirect gaps produced by alloys of similar Si/Sn ratios. We find also that, unlike the Si/Ge layered superlattices, which tend to fold states from one coordinate direction and produce indirect-gap systems, multiple band folding increases the band repulsion at Γ, creating a direct gap even for the Si/Ge ordered alloy. Accordingly it would appear that simple direct-gap materials based on the group IV elements can be found that are composed primarily of Si. They do require far more complex growth methods than are currently used for Si/Ge layered SL's, but the benefit is the possibility of a silicon-rich system directly coupling to light. As a great deal of work has been accomplished with the growth of thin layers of Ge and Si, it would make an ordered 2×2 surface deposition of Ge the next evolutionary step towards an ordered alloy. Progress on Sn

deposition would also allow find tuning of the band gap either alone or in combination with Ge to form ternary ordered alloys. Carbon alloys based on Si(100) appear so far to be unsatisfactory for creating direct-gap materials although more work could be done on new real space geometries.

ACKNOWLEDGMENTS

This work was supported by the Semiconductor Research Corporation at Cornell University. We would also like to thank Professor Michael Teter for helpful discussions and for the use of the Corning Planewave Code.

[1] *Numerical Data and Functional Relationships in Science and Technology*, edited by K.-H. Hellwege, Landolt-Börnstein Tables, Group III, Vol. 17a (Springer, New York, 1982).
[2] M. S. Hybertsen and M. Schlüter, Phys. Rev. B **36**, 9683 (1987).
[3] S. Froyen, D. M. Wood, and A. Zunger, Phys. Rev. B **37**, 6893 (1988).
[4] J. M. Bass and C. C. Matthai, J. Phys. Condens. Matter **2**, 7841 (1990).
[5] C. Tserbak, H. M. Polatoglou, and G. Theodorou, Phys. Rev. B **47**, 7104 (1993).
[6] M. A. Gell, Phys. Rev. B **38**, 7535 (1988).
[7] S. Krishnamurthy, A. Sher, and A.-B. Chen, Phys. Rev. B **33**, 1026 (1986).
[8] J. L. Corkill and M. L. Cohen, Phys. Rev. B **47**, 10 304 (1993).
[9] B. Edwards and N. W. Ashcroft (unpublished).
[10] A. P. Horsfield and N. W. Ashcroft, J. Phys. Condens. Matter **4**, 7333 (1992).
[11] A. A. Baski, J. Nogami, and C. F. Quate, Phys. Rev. B **43**, 9316 (1991).
[12] J. Nogami, A. A. Baski, and C. F. Quate, Phys. Rev. B **44**, 1415 (1991).
[13] A. A. Baski, C. F. Quate, and J. Nogami, Phys. Rev. B **44**, 11 167 (1991).
[14] D. H. Rich, T. Miller, A. Samasavar, H. F. Lin, and T. C. Chiang, Phys. Rev. B **37**, 10 221 (1988).
[15] P. Hohenberg and W. Kohn, Phys. Rev. **136**, B864 (1964).
[16] W. Kohn and L. S. Sham, Phys. Rev. **140**, A1133 (1965).
[17] M. P. Teter, M. C. Payne, and D. C. Allan, Phys. Rev. B **40**, 12 255 (1989).
[18] M. C. Payne, M. P. Teter, D. C. Allan, T. A. Arias, and J. D. Joannopulos, Rev. Mod. Phys. **64**, 1045 (1992).
[19] D. R. Hamman, M. Schlüter, and C. Chiang, Phys. Rev. Lett. **43**, 1494 (1979).
[20] M. Teter, Phys. Rev. B **48**, 5031 (1993).
[21] D. M. Ceperley and B. I. Alder, Phys. Rev. Lett. **45**, 566 (1980).
[22] R. A. Evarestov and V. P. Smirnov, Phys. Status Solidi B **119**, 9 (1983).
[23] 12 points were used for the tetragonal $S_{15}X_1$ alloys, 6 for the simple cubic Si_7Sn_1 alloy, 11 for the body-centered tetragonal Si_7Sn_1 alloy, 8 for the tetragonal $Si_{13}Sn_3$ alloy, and 6 for the Si_3Sn_1 alloy.
[24] M. T. Yin and M. L. Cohen, Phys. Rev. Lett. **45**, 1004 (1980).
[25] D. Stroud and H. Ehrenreich, Phys. Rev. B **2**, 3197 (1970).
[26] J. R. Chelikowsky and M. L. Cohen, Phys. Rev. B **14**, 556 (1976).
[27] A.-B. Chen, Phys. Rev. B **16**, 3291 (1977).
[28] A.-B. Chen, Phys. Rev. B **7**, 2230 (1973).
[29] K. C. Hass, B. Velicky, and H. Ehrenreich, Phys. Rev. B **29**, 3697 (1984).
[30] M. S. Hybertsen and S. G. Louie, Phys. Rev. B **34**, 5390 (1986).
[31] R. W. Godby, M. Schlüter, and L. J. Sham, Phys. Rev. B **37**, 10 159 (1988).
[32] S. Fahy, K. J. Chang, S. G. Louie, and M. L. Cohen, Phys. Rev. B **35**, 5856 (1987).
[33] X. Zhu, S. Fahy, and S. G. Louie, Phys. Rev. B **39**, 7840 (1989).